Use of fiber reinforced concrete in bridges – Metrorrey Line 2 case study

Magí Domingo , Gonzalo Ramos [*] , Ángel C. Aparicio

Civil and Environmental Engineering Department (ETSECCPB), Universitat Politècnica de Catalunya BarcelonaTECH (UPC), C/Jordi Girona 1-3, 08034 Barcelona, Spain

ARTICLE INFO

ABSTRACT

An assessment concerning the structural applicability and performance of fiber reinforced concrete (FRC) is presented for different bridge elements and within a design framework. FRC as the main bearing material in structural members has evolved from low-demand applications to increasingly ones, where bending and shear are the main internal forces. In actual applications, this was reflected with initial slab-on-grade cases, through tunnels, and later moving towards elevated slabs. Past experiences show that FRC has notable features regarding ultimate capacity and serviceability performance (i.e., enhanced crack control). These capabilities allowed for optimizations such as material savings, reduction of intensive labor during construction, or extended durability. Considering FRC's enhancements from previous applications, a case study based on the Metrorrey Line 2 light-train viaduct (Mexico) is developed. The case study aims to assess the structural performance that FRC can deliver within bridge geometries, loads, and specific conditions. Two numerical models considering different transversal post-tensioning configurations are developed based on the reference structure. The use of these two numerical models aims to broaden the applicability of this study to most U-shaped light-train viaducts. The design is based on current and future standards and recommendations, being prEN1992-1-1:2021, EN1992-1-1:2004, and *fib* Model Code 2010. After the numerical models and structural analysis, different sectional analyses at ultimate and serviceability levels are carried out, considering both conventional and fiber reinforced concretes. From the sectional results, FRC can provide reductions to reinforcement quantities at ultimate load levels, which are tied to the initially required reinforcement ratio (in other words, linked to the internal forces existing in the element). When higher reinforcement ratios are necessary, FRC optimizations point toward serviceability limit states, especially on the crack width reduction and the potential to reduce or suppress any additional reinforcement due to crack limitations.

1. Introduction

Fiber Reinforced Concrete (FRC) is a concrete-based material made of conventional concrete combined with randomly distributed (and oriented) short fibers, which are homogeneously added during its mixing. Adding fibers to concrete improves one of its significant shortcomings, the low/insignificant post-cracking ductility traditionally addressed with rebar reinforcement [1]. Fibers increase the concrete toughness and allow it to sustain tensile strength even after the crack has appeared by uniformly bridging the two sides of a crack plane. The extent of its bearing capacity will depend on the fiber amount and characteristics together with concrete properties. Several publications have covered the evolution and current state of the FRC features, common fiber materials, and its present applicability to structural members [1–6]. Although several different fiber materials are used nowadays,

Steel Fiber Reinforced Concrete (SFRC) has been and still is one of the most used types of FRC. Current design recommendations and codes were derived from SFRC research, and they mainly target this material in their design formulations. It is the material on which this paper will be focusing. From here on, SFRC will be indistinctly called FRC unless specified.

Like many materials and technologies, FRC has been gradually introduced into structural applications, most probably due to an initial lack of knowledge, difficulties in using recommendations, and insufficient proof of its performance. Fibers as main reinforcement have shown a pattern from low internal forces requirements to higher ones, where bending and shear are the main design forces. This matches how real case applications have evolved, from early usage on slabs-on-grade (with very low demands) to precast tunnel segment linings (compression under service and a relatively low bending and concentrated loads

during construction phases), to one of the latest use cases, elevated slabs (bending and shear are the main design forces). Recent experiences with FRC elevated slabs from real-world applications and research campaigns showed that fibers can effectively replace all (or almost all) conventional reinforcement despite the increase of internal forces compared to initial slab-on-grade loads [7–9].

FRC has also proven very beneficial to the shear behavior of concrete beams and slabs, including cases with and without shear reinforcement [10], with large dimensions [11], and/or with prestressing steel [12,13].

In addition to the mechanical improvements that fibers can deliver, a well-formulated FRC can be very effective at crack control and arrestment, providing an enhanced serviceability performance and extended durability [1,14,15]. However, it is paramount to understand how FRC performs in outdoor environments and in terms of the material degradation itself, becoming especially true in bridges, where high chloride environments are not uncommon (de-icing salts, marine environment, etc.).

Moreover, a well-grounded understanding of FRC concerning its interaction with reinforcement and its protection is needed. Nevertheless, reduced long-term knowledge of FRC structures exists, which might be an additional reason that prevents further use of it in large civil infrastructures [15,16].

The use of FRC in bridges has been more discrete compared to other structural fields. Mufti et al. [17] did one of the earliest studies regarding the use of FRC in bridge elements. They tried to entirely eliminate the steel reinforcement from the concrete decks in beam-and-slab bridges. This was possible as the ultimate resisting mechanism of the slab is an arch within it if transversely restrained. In their proposal, they used bottom steel strips. One of the goals that pushed for the complete suppression of steel reinforcement was its high probability of corroding, subsequently affecting the structure's durability. Further research focuses on different configurations of beam-and-slab elements made of FRC and UHPFRC (Ultra High-Performance FRC). From the predesign proposed in [18], steel fibers had an important contribution to ultimate shear capacity and to the enhanced ductility they provided at bending and shear. From [19], it was seen that using SFRC in bridge decks enhanced their performance in terms of service and ultimate states. Steel fibers allowed the reduction of the conventional reinforcement amount while keeping the same safety levels.

There are more recent investigations from McMahon et al. [20,21] regarding SFRC in concrete decks of beam-and-slab bridges. They showed that, at ultimate levels, the failure capacity of the deck significantly increased. At service states, the steel stress was reduced compared to the design reference values, thus, increasing the allowable service moment or enabling a reduction of the serviceability reinforcement.

A real-case application of FRC in long-span bridges is found in [22]. FRC was used in the web design of the butterfly web bridges. Although FRC was not instrumental in the shear resistance of the precast members (the tensile cord of the double-warren truss was controlled by prestressing strands), it did ease the creation of the web itself. The panels did not present any reinforcement (even non-structural, such as skin reinforcement). Hence, it allowed the thickness reduction of the web to the minimum required for the compression strut to resist, optimizing the concrete volume of the web. Consequently, all procedures and designs depending on the superstructure self-weight were optimized, such as the substructure bearing capacity [23].

Another recent experience is a frame bridge built with self-compacting concrete and using fibers in Denmark [24]. It was found that some reinforcement could be omitted from all members (deck, walls, and foundation). If using FRC, the bending capacity of the deck was improved from 6 to 40% compared to a conventional reinforcement solution. Crack width improvements ranged between 23 and 26%. Shear strength in the deck was increased between 53 and 75%. Additional reinforcement required to control shrinkage cracking was also omitted by using FRC.

From past experiences, FRC has allowed the optimization of different parameters that influence the design of structures, from ultimate bearing capacity to improved durability. Those optimizations could be shaped into reinforcement reductions, a decrease in placement labor, a reduction of the crack widths, or a reduction of rebar congestion due to durability-specific reinforcement, among other possible advantages.

This investigation aims to study the structural implications of SFRC on the design of the bridge superstructure, accounting for all previously mentioned potential benefits. Especially focusing on its influence on the reinforcement requirements for the main resisting elements to fulfill both ultimate and serviceability limitations. The assessment is done through a case study based on an existing structure, in which geometric and reinforcement details are known (and not discussed). The main elements of the bridge are re-designed considering FRC with several design residual strengths and later compared to the previous conventional solution. The design is limited to current codes and standards, trying to capture FRC influence for future designs, and hence, avoiding tools and material definitions that lay far from common practice.

2. Bridge description, modeling, and design considerations

The bridge considered for this case study is the Metrorrey Line 2 extension viaduct, part of the urban rail system of Monterrey (Nuevo León, Mexico). The viaduct was completed between 2007 and 2008, and its final design (as it changed from the initial proposal) was developed by Juan José Goñi Baamonde from Garcia Bridge Engineers [25]. It consists of simply supported girders made of wide U-shaped precast segments (reassembling a half-through girder). A novel aspect of the viaduct design was the use of transversal prestressing together with the conventional longitudinal one combined with the U-shaped cross-section. The use of transversal post-tensioning allowed for very reduced reinforcement quantities in the transversal direction and an important contribution to resist longitudinal shear. Compared to other solutions, this led to material usage and workforce optimizations [25]. The reduction levels achieved in the existing structure due to transversal prestressing is one of the reasons that motivated its use in this case study.

Beyond the existing Metrorrey Line 2 viaduct, wide U-shaped girders are becoming increasingly popular for light-rail mobility systems. Some recent examples are the Metrorrey Line 3, Mumbai Metro Line 7, and the Dubai Expolink 2020 viaducts. Because of the rise in popularity, this paper also extends the assessment of FRC to wide U-shaped concrete bridges with longitudinal post-tensioning while only ordinarily reinforcement is placed in the transverse direction. This expands the present study and makes it valid for most of the wide U-shaped light-train viaducts and not only the cases where transverse post-tensioned solutions are used. The details and procedures to define the additional cases are presented in Section 2.4.

2.1. Viaduct properties and description

The Metrorrey Line 2 viaduct properties presented herein are obtained from [25], where the reader can get further and complementary details. The most relevant information for the modeling and verification is included for convenience.

The existing viaduct consists of simply supported U-shaped post-tensioned precast segmental girders with an approximate length of 37 m and a span of 34.93 m. Each girder comprises two 2.49 m segments located above the piers and nine 3.55 m long segments. The typical segment is made of a single concrete shell with a constant depth of 0.3 m in the webs and ranging from 0.3 to 0.25 m in the bottom slab. The bottom slab is 0.6 m deep in the segments above the piers to accommodate the internal forces that flow from the webs to the bearings. The height of the girder, including the two prominent compression blocks, is constant and with a value of 1.9 m. The typical span presents three types of post-tensioned systems: (1) main longitudinal bonded post-tensioned tendons placed at the bottom slab, (2) longitudinal bonded post-tensioned tendons at the compression chords (to counteract negative
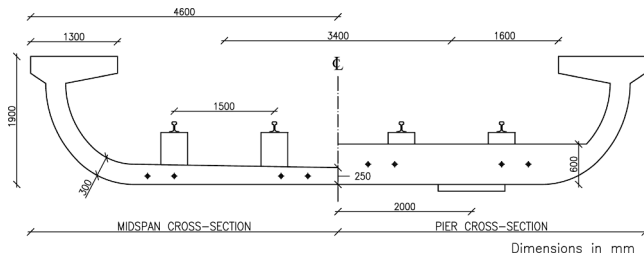
Fig. 1. Cross-section of the reference bridge at midspan and piers. Dimensions obtained from [25].

bending moments at supports due to main longitudinal tendons), and (3) transversal unbonded post-tensioned greased mono-strands. Fig. 1 presents a schematic drawing of the midspan and pier cross-sections.

2.2. Code and recommendation baselines, design loads, and used tools

Although the Metrorrey viaduct was designed based on American standards, the reference design codes used in the subsequent verifications are the Eurocodes 1 and 2, more specifically EN1991-2:2003 [26], EN1992-1-1:2004 [27], and prEN1992-1-1:2021 [28] which will be referred as EC1, EC2:2004, and EC2:2021 respectively. In addition, *fib* Model Code 2010 [29,30] recommendations are also considered, referred to as MC2010. Regarding EC2:2021, as it is still a pre-normative document under discussion, some of the definitions might not be consistent in the eyes of the authors. Those are complemented either with MC2010 or alternative expressions from the literature. This is the case concerning the shear expressions when requiring transversal reinforcement (see more details in Section A.3).

Table 1 shows the values of the most relevant parameters considered in the design of the studied bridge. From this table, it must be noted that: (1) additional/different load factor values are assumed from reference code EC1 as it does not apply by itself to light-train bridges, and (2) only gravitational loads are considered as these govern most of the internal forces regarding FRC design, and they allow certain simplicity during the modeling and structural evaluation.

SAP2000 v21 (CSI, [32]) is used to define the different numerical models and obtain the internal forces for later verifications. In addition, a self-developed program for computing the cross-sectional equilibrium is used. This program is based on the Euler-Bernoulli beam theory (plane deformations) and the assumption that conventional reinforcement and bonded post-tensioned tendons show perfect adhesion with the surrounding concrete (strain compatibility). It allows using any material constitutive law and cross-section shape, as they are discretized by layers (only allows for unidirectional bending). The main algorithm
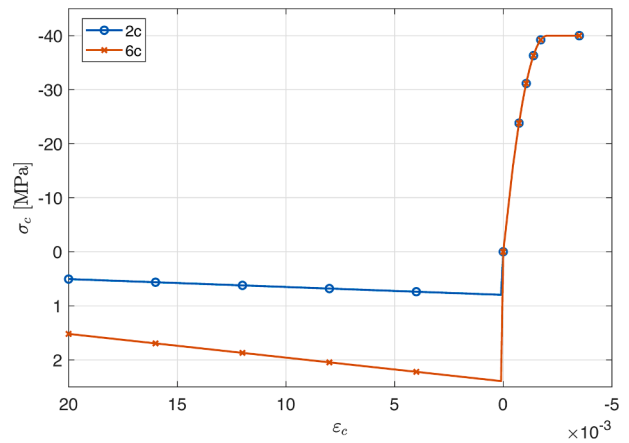

Fig. 2. Constitutive law for FRC with 2c and 6c strength classes. Note the scale change in the stress axis to explain the change in the modulus of elasticity. $\sigma_c < 0$ refer to compression.

seeks the curvature and bottom strain that ensures equilibrium given an axial load and bending moment. Auxiliary algorithms look for the efficiency of the cross-section, minimum reinforcement, and curvature-moment relationships.

2.3. Material definition

The segments are assumed to be cast with C40 concrete and with different fiber scenarios. It includes a conventional (non-FRC) configuration and different residual strength SFRC classes, as materials are compared to each other along the paper. One of the objectives is to assess SFRC from a design framework. Thus, all material parameters are obtained from current design codes EC2:2004 and EC2:2021 (unless otherwise specified). To simplify the SFRC residual strength influence assessment, only class "c" FRC's are used (according to EC2:2021, $f_{R3,k} = 0.9 f_{R1,k}$), while $f_{R1,k}$ ranges from 2 to 6 MPa (concrete residual strength at CMOD = 0.5 mm). For instance, a 2c strength class would be defined as $f_{R1,k} = 2$ MPa and $f_{R3,k} = 0.9 \cdot f_{R1,k} = 1.8$ MPa.

A reference length is needed to transform crack widths to post-cracking strains, the characteristic length. Following the EC2:2021 Annex L simplified assumption, a constant characteristic length of 125 mm has been considered throughout this investigation. However, this assumption might lead to a slight overestimation of the concrete strength given a strain in certain cases. This is not dealt with in this paper.
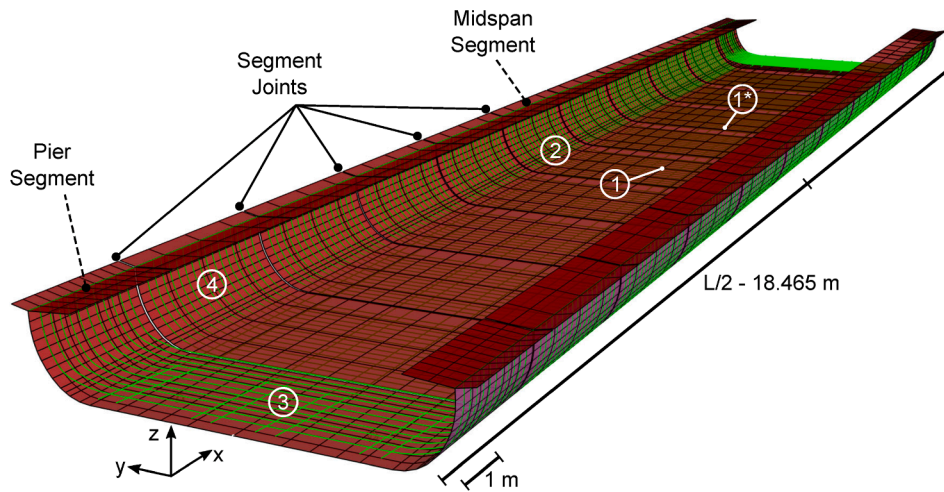
Table 1
Most relevant design parameters considered in the numerical model and sectional verifications.

	Description	Value
Basic design parameters	Service life and exposure class	100 years in XS1 environment
	Equilibrium strains and crack design limitations	$\varepsilon_c = 3.5‰$ (ULS concrete compression)
		$\varepsilon_s = 10‰$ (ULS steel tension)
		$w_k \leq 0.2$ mm (Crack width requirement after [31])
Load values	Dead load	25 kN/m³
	Superimposed dead load	5.03 kN/m per rail
		1.25 kN/m² (across all horizontal slab)
	Live load	Defined as per [25]
Load factors (after EC1)	Specific bridge load combination multipliers	$\alpha = 1.25$ classified vertical loads
		$\varphi = 1.15$, dynamic amplification (longitudinal verifications)
		$\varphi_T = 1.465$, transversal dynamic amplification (transversal verifications)
		$\psi = 0.8$, accompanying load multiplier (second train)
	Partial safety load factors	$\gamma_G = 1.35$ for permanent loads
		$\gamma_P = 1$ for post-tensioning actions
		$\gamma_Q = 1.5$ for live loads.

Fig. 3. Numerical model of the simply supported girder, including longitudinal and transversal prestressing (Metrorrey case, wPT model). "L" defines the overall girder length and 1 m is the distance from the edge of the girder to the center of the bearing pad.
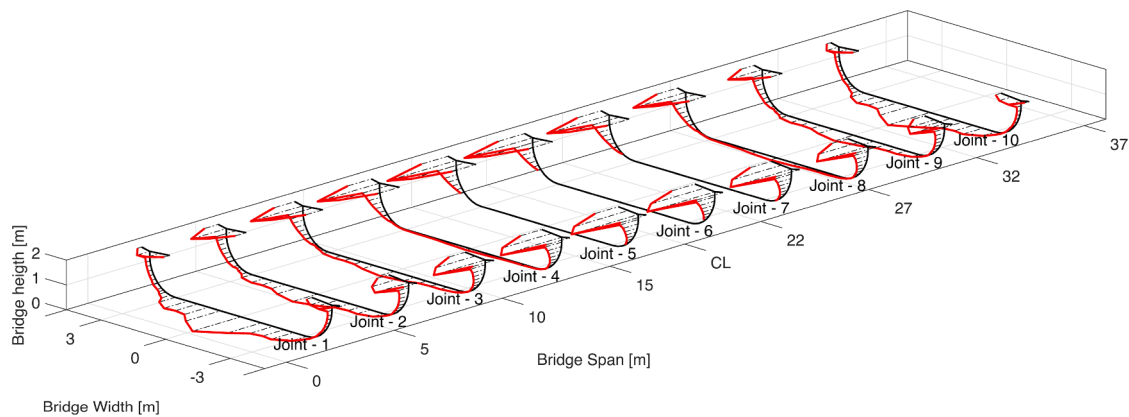

Fig. 4. Compressive internal forces along the segment joints at ULS and under two train load. Black lines represent the joint mid-plane meanwhile red lines represent the axial load through the joint (zero load does not have representation). (For interpretation of the references to colour in this figure legend, the reader is referred to the web version of this article.)

From Fig. 2, a parabola-rectangle law for compression and a linear relationship for tension are used to define the constitutive behavior of concrete (see Section A.1 for the definition of the constitutive law in tension). From the previous constitutive law, concrete under tension will never reach the ultimate strain in the presence of reinforcing steel as its design strain is lower. In addition, EC2:2021 includes an orientation factor, κ_O, that ideally compares the fibers' orientation in the final element to the fiber orientation from the material characterization test (three-point bending, round slab, or any considered standardized test) and its effect on the strength. It reduces the material capacity if fiber orientation is detrimental to the final mechanical behavior compared to the tested casting. From the experimental campaign by Aidarov et al. [9], fibers showed an orientation distribution such that about 40–50% of them contributed to each main direction of the tested slab. In addition, a non-homogeneous distribution of fibers along the depth was observed in the same slab. This would justify using $\kappa_O = 0.5$ in this paper, in addition to 1, to consider different casting scenarios and their influence on the structural performance.

The reinforcement used in the sectional analysis is a B500SD type with an elastic–plastic design constitutive law and 200 GPa elastic modulus. The post-tensioning steel is a Y1860 type with an elastic-hardening design constitutive law and 195 GPa elastic modulus. Both materials are defined according to EC2:2004.

2.4. Numerical modeling of the typical girder

Two numerical models are defined to capture the two cases proposed earlier in this section, a conventional wide U-shaped girder for light-trains (without transversal post-tensioning) and the Metrorrey girder itself (with transversal post-tensioning). The numerical models start from the same Metrorrey girder geometry, materials, and loading definitions but consider different approaches concerning the transversal post-tensioning. Thus, two identical models are created with the only difference that transverse post-tensioning exists/does not exist. The case including the transversal tendons will be referred to as "wPT" (with Post Tensioning, representing Metrorrey viaduct). The case without transversal tendons, replicating a generic U-shaped girder, will be referred to as "woPT" (without Post Tensioning).

The models are geometrically defined through 2D elastic shells representing the mid-plane of the U-section for a single girder. See Fig. 3.

Since it is a precast segmental bridge, transversal joints are modeled so that internal forces are transmitted only when the joints are under compression. This implies that not only compression but also shear forces are transferred only if joint contact exists, reassembling to a dry joint. The numerical element used to reproduce such behavior is the *Friction-Pendulum Isolator* from the software catalog with the particularity of using infinite pendulum radius to model a flat surface (see more details in [32]). To improve numerical convergence, in areas where it is
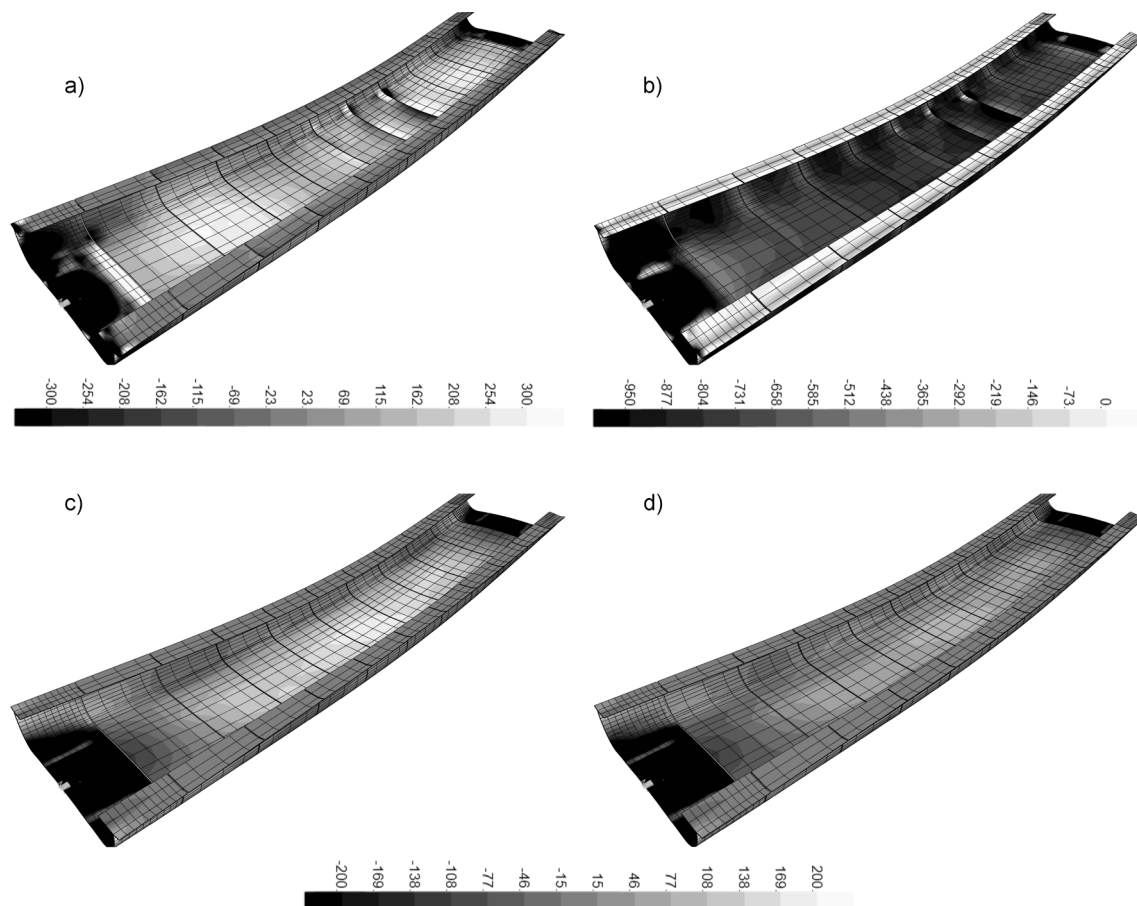
Fig. 5. Shell internal forces due to ULS load combination, considering two light-trains running in opposite directions and the center of the trains at midspan. Figures (a) and (b) correspond to axial internal forces from woPT and wPT models, respectively. Figures c) and d) correspond to the bending moment loads for woPT and wPT models, respectively. All units in kN/m and kNm/m when appropriate.

known beforehand that compressions will occur, no matter the load combination (e.g., compression chord in midspan), the nonlinear links between nodes are replaced by rigid ones.

Regarding the longitudinal and transversal post-tensioning system, tendon areas of 2550 mm², 900 mm², and 140 mm² are considered for each bottom and top longitudinal and transversal tendons, respectively, and following [25]. The tendon layout of the bottom longitudinal post-tensioning is straight and centered at mid-height of the bottom slab with slight upward bends at the pier segments to accommodate the post-tension anchorage system (Fig. 3). The transversal post-tensioning layout follows the U-shape of the cross-section. The tendons are centered at the webs and eccentric at the bottom slab to provide adequate bending moment action. The final stress is assumed to be 65% of the ultimate stress for all types of tendons and after all losses.

3. Results from the bridge structural models

After defining the numerical models, including the load assumptions and hypothesis introduced in Section 2, the internal forces are obtained and later used for checking the most representative elements (as discussed in Section 4). The most relevant results of the modeling are shown in this section.

Internal forces of the girder are longitudinally and transversally uncoupled and follow the principal directions of the girder elements (beam behavior in the longitudinal direction and slab behavior in the transverse one).

Concerning the overall longitudinal bending, both numerical models (woPT and wPT) render very close results, as longitudinal and trans-

versal behavior are almost uncoupled. The design bending moment (ULS) of the girder is 35.8 MNm (entire cross-section). Under design loads (ULS) the maximum concrete stress is 22.6 MPa, or equivalently, a compressed block of 27.6 MN. The longitudinal post-tensioned tendons show average tensile stress of 1260 MPa. The cross-section efficiency at the ULS level is 0.8 (computed as M_{Ed}/M_{Rd}, design bending due to actions and resisting mechanism respectively), and the concrete under compression is the first to reach the ultimate strain meanwhile the post-tensioned tendons reach a stress of 1468 MPa. As the neutral axis depth is relatively high, internal force increments yield to rather low prestress strain increases (thus, low stress increases). Segment joint separation is expected between the central segments, at joints 5 to 7 (see Fig. 4), as the load between the joints drops to zero in the bottom slab. Under the SLS load combination, a fully compressed stress field is obtained with concrete compressive stresses ranging from 17.3 MPa (43% of f_{ck}) to 2.6 MPa from the top to the bottom fibers, respectively.

Oppositely to longitudinal bending results, the effect of transversal post-tensioning outcomes in different internal forces in the bottom slab depending on the existence or not of the transversal tendons. Fig. 5 shows both axial force and bending moment in the transverse direction. The results correspond to a ULS load case including two light-trains running in opposite directions (specifically when the center of each train is at midspan) and combination coefficients as defined in Section 2.2. Thus, the values do not correspond to an envelope, although they represent the maximum values.

From the graphical results, it can be seen how transversal post-tensioning can reduce the final bending moment of the slab by 50% from the non-prestressed counterpart. This fact is relevant for the FRC

Table 2

Internal forces and location (according to Fig. 3) for the design check of the bottom slab in the transversal direction. Internal forces for sections not checked are not shown.

Case	Location	ULS		SLS	
		N [kN/m]	M [kNm/m]	N [kN/m]	M [kNm/m]
woPT	1	217.17	188.8	154.6	133.8
	3	−95.2	−1084.8	−8.7	−781.4
wPT	1	−701.4	105	–	–
	1*	−405.41	99	–	–
	3	−1393.4	−1174.6	−1306.4	−870.9

Table 3

Reinforcement layout proposal and required steel area per unit width for each design case and for a typical cross-section (no local effects) considering conventional concrete (without FRC).

Case	Reinforcement proposal per unit width (Min A_s [cm^2/m])			
	25 cm woPT	30 cm woPT	35 cm woPT	25 cm wPT
Bottom – ULS	6∅25 (26.81)	5∅25 (21.17)	4∅25 (17.82)	4∅12 (3.61)
Top – ULS	6∅20	5∅20	4∅20	4∅12
Bottom additional reinforcement – SLS	+2∅25	+2∅25	+2∅25	–

implementation and use in the viaduct.

In addition, localized axial internal forces appear at the edges of central segments Fig. 5a and Fig. 5b) due to segment joint separation at ULS. These forces become relevant for the wPT case and will be considered during the wPT slab design check.

Finally, it should be recalled that prestressing loads are already included in the model. This is relevant for the transversal post-tensioning action, as the cross-sections to be verified will include it in the resulting bending moment and axial load from the numerical model. Hence, the tendons are not explicitly considered in the sectional definition. Given the unbonded nature of the tendons and their complicated layout around the girder, their current modeling makes their prestressing action to be adequately captured in the global analysis.

4. Design of structural members

The main objective of this paper is to assess the structural influence of FRC on the different elements of the Metrorrey Viaduct. This evaluation is done by comparing reinforcement requirements to fulfill both ULS (ultimate strain) and SLS (crack width) from the most representative members of the viaduct. Those are designed considering a conventional solution and are later re-designed including the influence of fibers, and the results are compared afterward.

The "ULS reinforcement" and "SLS reinforcement" are the measures used during the comparisons. The "ULS reinforcement" is defined herein as the minimum theoretical mechanical amount of reinforcement that is required to achieve the cross-sectional equilibrium with an efficiency equal to 1 under combined axial-bending loads, either while using FRC or not. The theoretical amount is defined as the reinforcement area per unit width (cm^2/m) and does not necessarily match the reinforcement placed in the actual bridge. The "SLS reinforcement" is the required reinforcement to fulfill the serviceability crack width limitations. It is obtained iteratively until a satisfactory crack width is obtained while minimizing the reinforcement amount. The design conditions and limitations are the ones defined in Section 2.2.

Before any in-depth analysis, the longitudinal bending design of typical prestressed concrete girders might hardly be influenced by the addition of fibers. This is especially true if precast segments are used or the beams are cast in several phases (i.e., cantilever construction

methods). In those cases, the joints eliminate the material continuity that it inherently requires to stand any mechanical influence. To that matter, segmental bridges rely solely on post-tensioning when assessing ULS cases. In addition, under SLS combinations, many post-tensioned bridges are designed to exhibit fully compressed cross-sections. Thus, no cracking appears during serviceability (and fibers are not enabled then).

Oppositely, longitudinal shear might benefit from the use of FRC, as well as the bottom slab in the transversal direction (as there is material continuity). Therefore, the design checks will be narrowed down to bending of the bottom slab (Sections 4.1 and 4.2) and shear of both the bottom slab in the transversal direction and the girder in the longitudinal direction (Sections 4.3.1 and 4.3.2).

The sections' positions to be designed are shown in Fig. 3 and are referred to with different numbers. Those are: (1) bottom slab at midspan (bending design), (1*) bottom slab segment edge (local bending design) after Joint 7 (see Fig. 4), (2) intersection of the bottom slab and web at midspan (transversal shear design), (3) bottom slab over piers (bending design) and (4) webs near supports (longitudinal shear design). The corresponding cross-section properties (depth and reinforcement) are defined in subsequent paragraphs.

Table 2 shows the internal forces considered during the design checks for the transversal bending of the bottom slab. These internal forces are obtained from ULS envelopes (considering one and two trains, no trains, etc.) and include the corresponding transversal dynamic amplification factor. The design checks are done per unit width. From Table 2, and as earlier mentioned in Section 3, cross-section (1*) is only verified within the wPT case and only exists when segment joint separation takes place, thus, no SLS verification for the (1*) cross-section will be done. Similarly, cross-section (1) is not verified under SLS combination as tensile stresses remain in the elastic regime.

The bottom slab without post-tension and at midspan is designed considering several slab depths (see Section 4.1). Despite the different depths, it is assumed that the same internal forces obtained for the initial woPT model (slab thickness of 25 cm) apply to other slab depths, disregarding any slight self-weight increase due to depth increment.

4.1. Transversal flexure of the bottom slab – Midspan segment

The bottom slab design consists of 25 cm element for the wPT case and different slab thicknesses for the woPT case, namely 25, 30, and 35 cm. Such slab variation in the woPT case is justified as 25 cm is not a common design depth for non-prestressed slabs, although it is kept as it is the reference slab for the Metrorrey viaduct. For low slab depths, reinforcement quantities would rapidly rise compared to higher depths. The reinforcement mechanical center is placed at 50 mm from the concrete surface in all sectional analyses. This is consistent with a concrete cover limitation of 35 mm regarding durability in an XS1 environment.

Table 3 shows the conventional "ULS reinforcement" for both the woPT and wPT cases (in parentheses cm^2 per unit width), together with their possible reinforcement layout. It also shows the serviceability requirements to fulfill the crack width limitation, which for all woPT cases results in a supplementary reinforcement of 2∅25 over the ULS reinforcement.

The theoretical ULS reinforcement obtained for the wPT analysis case is 3.61 cm^2/m. This result is consistent with the reinforcement of the existing Metrorrey Line 2 structure (#3 rebar every 220 mm ≈ 3.24 cm^2/m [25]).

4.1.1. ULS verification with FRC

It is possible to reduce the initial "ULS reinforcement" in all design cases if FRC is considered for ultimate verifications. From Fig. 6, the reinforcement reduction varies according to the depth of the element, the overall internal forces (which are tightly related to transversal post-tensioning existence), and the orientation factor. It is relevant to notice
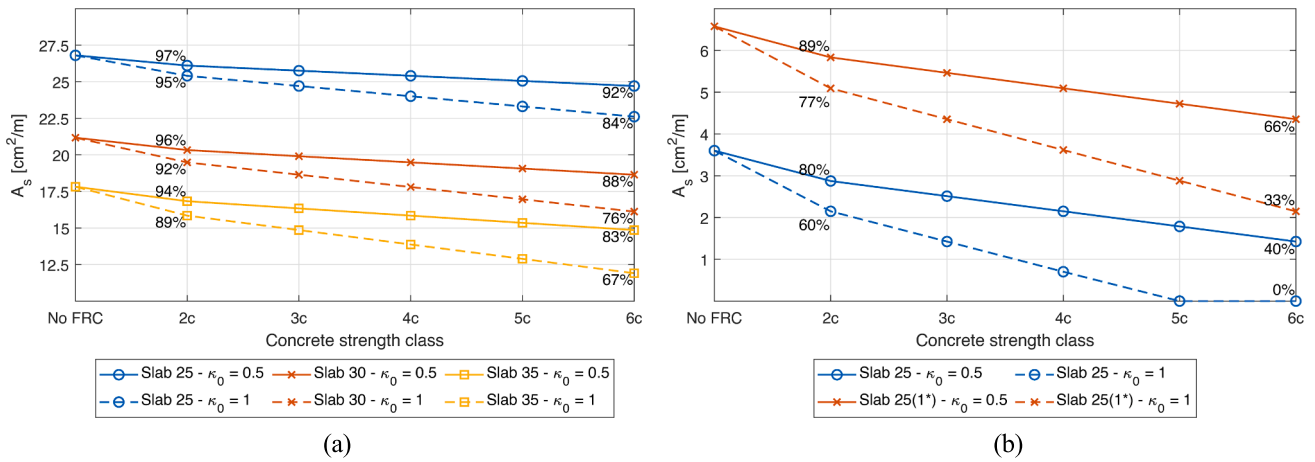
Fig. 6. "ULS reinforcement" depending upon FRC strength class and fiber orientation factor (κ_O). Results for (a) woPT case and (b) wPT case. The reinforcement reduction percentages are shown relative to the initial "No FRC" reinforcement (see Table 3) and consider the same performance requirement between cases. Intermediate reduction values can be interpolated from the ones shown.
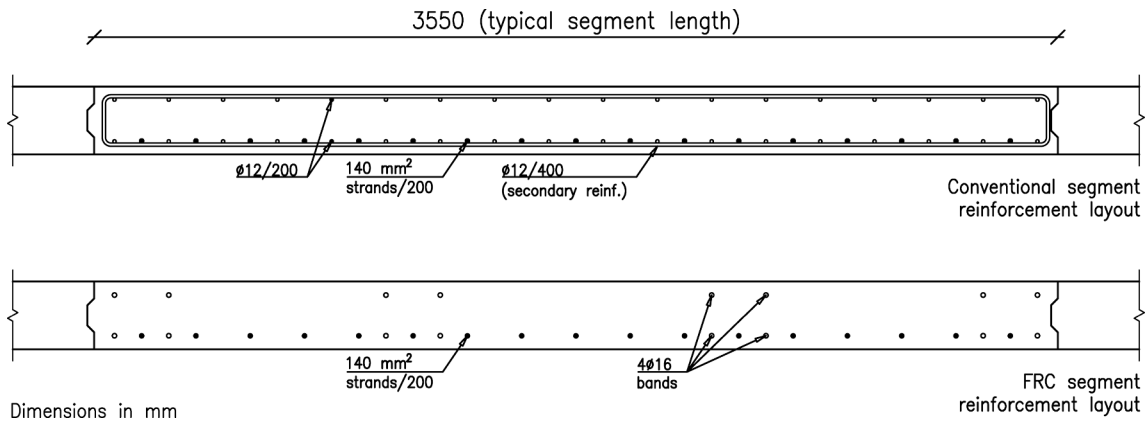

Fig. 7. Transversal bottom reinforcement layout proposal for the Metrorrey typical segment (3.55 m). Transversal section-cut view.
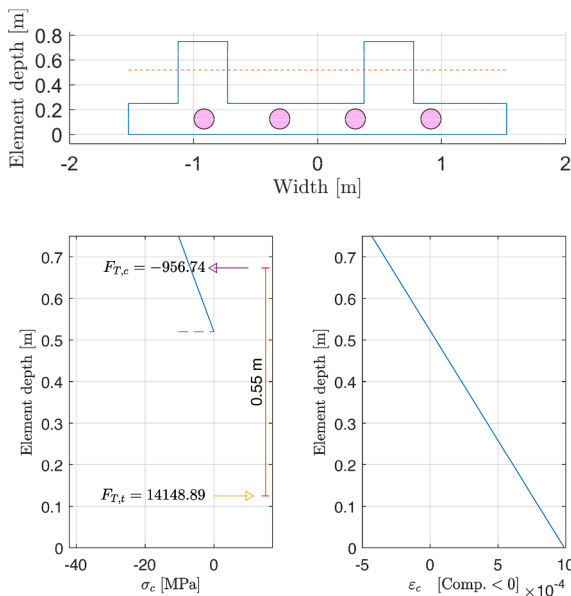

Fig. 8. Bottom half-slab cross-section with plinths under longitudinal bending. Stress and strain profiles under ULS loads and material coefficients. *Note: Stress integration forces in kN.*

the linear relationship that exists between the FRC strength class and the ULS reinforcement reduction independently of the slab depth or the post-tensioning. This would provide means for a quick assessment and extrapolation of any FRC strength class or orientation factor (which modifies the design strength at the end) for a given cross-section and a known point of the line.

From Fig. 6b the complete elimination of ULS reinforcement could be achieved from the FRC 5c class and beyond with a favorable orientation factor. However, the reinforcement reduction (or elimination) attained if FRC is used along with transversal post-tensioning (wPT case) could raise some concerns. Considering that:

- According to many standards and recommendations (e.g. [27,33,34]), minimum reinforcement should always be provided to prevent a sudden and brittle failure of the concrete member just after cracking. Such reinforcement should most preferably be bonded to arrest the crack growth effectively.
- EC2:2021 establishes that minimum reinforcement of beams and one-way slabs should never be replaced by fibers (only the secondary reinforcement in one-way slabs).
- At the segment edges of the wPT model, verification 1*, the "ULS reinforcement" requirement is still 2 cm²/m.

Despite EC2 allowing unbonded tendons to fulfill structural robustness if certain conditions are matched, the complete replacement of bonded reinforcement by fibers could be perceived by designers as a
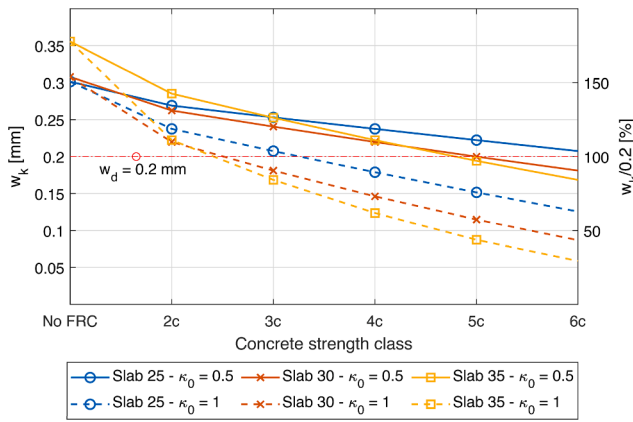
Fig. 9. Characteristic crack width depending upon FRC strength class and orientation factor while using the ULS initial reinforcement. *Note: w_d is the design crack width limit.*

reduction in structural redundancy. Consequently, a reinforcement reassembling the Anti Progressive Collapse (APC) reinforcement presented in [35] is proposed. As an example, the APC reinforcement was used in the experiments from Aidarov [9] as column ties, and it can provide a secondary load-carrying mechanism, as exposed in [35]. For this case, the APC reinforcement is defined as four bands of $2\varnothing16$(top) + $2\varnothing16$(bottom) rebars evenly distributed across the segment.

In Fig. 7 a simplified segment section-cut shows the final reinforcement proposal for 6c strength class concrete with the APC bands compared to the conventional segment. In addition to the structural fail-safe purpose of the APC bands, they also serve as the support needed during construction. It cannot be expected to entirely eliminate all the reinforcement if longitudinal and transversal post-tensioned tendons/ducts are to be set.

From Fig. 7, a relevant optimization, in terms of reinforcement and rebar placing labor, is the suppression of the longitudinal reinforcement in the bottom slab. As mentioned before, FRC does not play any significant role in the overall longitudinal bending resistance because of the segment joints. However, internal forces still need to be considered at each segment due to the local loading of the train while the wheel truck is over the segment itself.

From the previous structural analysis model for the woPT case and under the ULS combination, the internal longitudinal axial-bending forces for half bottom slab (as represented in Fig. 8) are [N, M] = [537.8 kN, 590.7 kNm]. Fig. 8 shows the stress and deformation distributions obtained for the ULS internal forces considering the ordinary concrete solution only with the bonded longitudinal tendons (without mild longitudinal reinforcement) and accounting for the plinths' flexural influence. It should be noted that plinths are assumed to be continuous within the segment and discontinuous to adjacent segments. All strains fulfill the ultimate strain criteria both for steel and concrete, thus, verifying the element under local longitudinal bending. This check implies that any additional reinforcement placed in the longitudinal direction is not mechanically necessary and makes it secondary. As EC2:2021 allows the complete elimination of the secondary reinforcement in one-way slabs, it would then make feasible the reinforcement layout from Fig. 7. All longitudinal reinforcement ($\varnothing12/400$) has been

eliminated and transversal reinforcement ($\varnothing12/200$) has been simplified.

4.1.2. SLS verification with FRC

The use of FRC also allows the reduction of the crack width, which could be reinterpreted as a possible reduction of the additional reinforcement necessary to control the crack width when fulfilling code limitations. Only the woPT case slabs are considered as these are the ones that crack under serviceability load combinations (for the wPT case, the concrete tensile stress is below f_{ctk}). From Fig. 9, concrete strength classes beyond 5c, even with an orientation factor $\kappa_O = 0.5$, prove to be effective at controlling crack width below code limits while only the corresponding ULS reinforcement for each slab depth (Table 3) has been considered.

From Fig. 9, the crack width reduction achieved with fibers goes beyond the limiting design value for higher FRC strength classes (i.e., 6c) and with unit orientation factor. The crack width, in this case, is around 50% of the design crack opening. Provided that there is some reduction margin in terms of ULS and SLS reinforcement, it would be reasonable to optimize the ULS reinforcement as well, and not only the SLS reinforcement. Table 4 shows the overall reduction that can be achieved by considering a reduced reinforcement amount for ULS design (from Fig. 6a) which still verifies the serviceability limitation. The FRC strength class considered for this case is 6c.

4.1.3. Fatigue verification (without FRC)

Several publications [36,37] highlight the performance of FRC in front of fatigue loading cases as being beneficial and with potential. However, FRC "fatigue" resistance cannot be considered in EC2:2021 design checks. In that case, the strength provided by the fibers should be disregarded when assessing the fatigue resistance in a cross-sectional analysis. In fact, Germano and Plizzari [38] consider that, depending on the fiber content, the additional flaws that fibers introduce into the concrete matrix outweigh the beneficial post-cracking strength obtained with them.

Consequently, the ULS reinforcement proposed in Table 3 is verified again as conventional concrete (without FRC) and under fatigue load. Only the woPT case is verified as wPT case does not crack under characteristic load combination. For sake of simplicity, only the 25 cm slab is considered. In Section A.2 more details about the design cycle count and limiting stresses are provided.

Table 5 shows the stress ranges in the reinforcement considering: 1) $8\varnothing25$ for the conventional slab solution and 2) $6\varnothing25$ for the FRC solution (as serviceability reinforcement has been suppressed). In both cases, stress ranges are below the limiting one (see Eq. (A4)), thus, fulfilling fatigue requirements. However, the stress gap from $\Delta\sigma_s$ to $\Delta\sigma_{Rsk}$ for the

Table 5
Design loads and reinforcement stresses due to characteristic loading (SLS) and self-weight (DL) with permanent loads (SDL).

Case	N [kN/m]	M [kNm/m]	σ_s[MPa] ($8\varnothing25$)	σ_s[MPa] ($6\varnothing25$)
DL + SDL	65.72	81.34	106	140
DL + SDL + LL (SLS)	130.97	116.16	187.4	246.8
$\Delta\sigma_s$			81	106.8

Table 4
Optimized reinforcement for the bottom slab of the woPT case. Including ULS and SLS FRC 6c class potential benefits.

Slab	Initially proposed reinforcement ULS/SLS	Min A_s – ULS [cm²/m]	Reinforcement proposal (Eff.)	SLS crack width verification [mm]	Reinforcement reduction [%]
25 cm	$6\varnothing25/+2\varnothing25$	22.61	$5\varnothing25$ (0.94)	0.14 (OK)	37.5
30 cm	$5\varnothing25/+2\varnothing25$	16.12	$4\varnothing25$ (0.87)	0.1 (OK)	42.8
35 cm	$4\varnothing25/+2\varnothing25$	11.9	$3\varnothing25/4\varnothing20$ (0.87/0.97)	0.077/0.09 (OK)	50

Table 6
Reinforcement layout proposal and required steel area per unit width for both ULS and SLS verifications considering the conventional solutions (without FRC).

Case	Reinforcement proposal (Min A_s [cm²/m]	
	woPT	wPT
Top – ULS	6⌀32	5⌀32
Bottom – ULS	6⌀20	5⌀20
Top additional reinforcement - SLS	+4⌀32	+3⌀32

FRC solution and the considered number of cycles is low, 5% margin compared to 28% for the conventional solution (gap calculated as $1 - \Delta\sigma_s/\Delta\sigma_{Rsk}$, being those the actual rebar stress range and the resisting stress range at 10^6 cycles).

4.2. Transversal flexure of the bottom slab – Pier segment

The pier bottom slab design consists of the 60 cm slab reinforcement verification (position 3 from Fig. 3). The main reinforcement is placed at the upper part of the cross-section as it endures hogging moments due to the web and bearings' relative position. It comprises ⌀32 rebars and their mechanical center is placed 60 mm from the concrete surface. Its position is consistent with the required concrete cover of 45 mm for an assumed XS3/XD3 environment for the pier slab. This environment is more restrictive than the bottom slab as direct water ingress from the top surface is possible in this case.

Table 6 shows conventional "ULS reinforcement" for both the woPT and wPT cases, together with a possible materialization of both required reinforcements and the serviceability reinforcement requirements.

4.2.1. ULS verification with FRC
Fig. 10a shows the ULS reinforcement (and indirectly the possible reinforcement reduction) when considering the use of FRC under ULS design. The results from woPT and wPT cases present a close behavior to the ones observed at the midspan bottom slab (Fig. 6a), but with greater reinforcement quantities as the bending moment demand is higher.

Although the minimum reinforcement is almost twice the required in the midspan bottom slab, the reduction percentages are somewhat similar. In [39], it was already seen that increasing resisting moments (which relates to increasing reinforcement quantities) led to decreasing

(a)

(b)
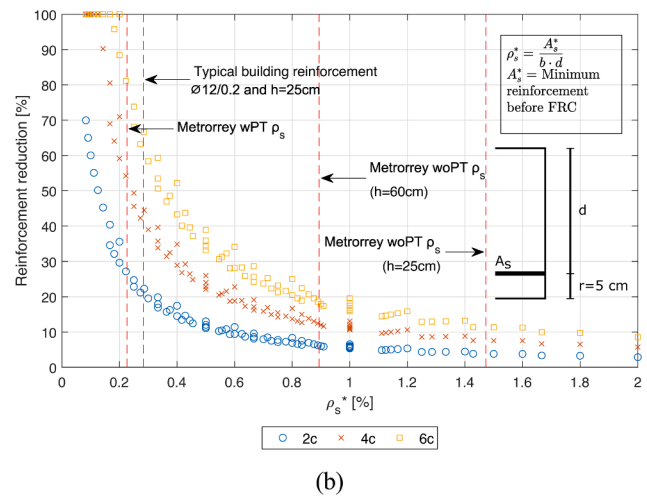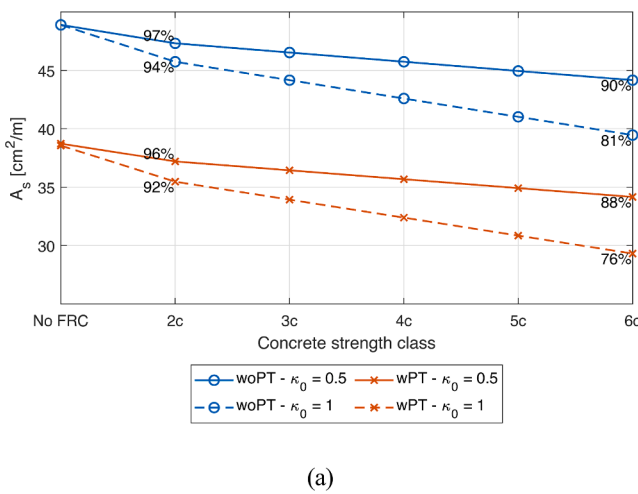
Fig. 10. Effect of FRC on ULS reinforcement reduction. (a) Reinforcement reduction depending on concrete strength class for ULS load combination at the slab over the pier (h = 60 cm) and considering the same performance requirements between cases. (b) Relationship between ρ_s^* and reinforcement reduction $(1 - A_{s,FRC}/A_s^*)$. *Notes: h = d-5 cm, b = 1 m, $\kappa_O = 1$ and A_s^* is the reinforcement amount with traditional concrete assessment (before FRC).*

(a)

(b)
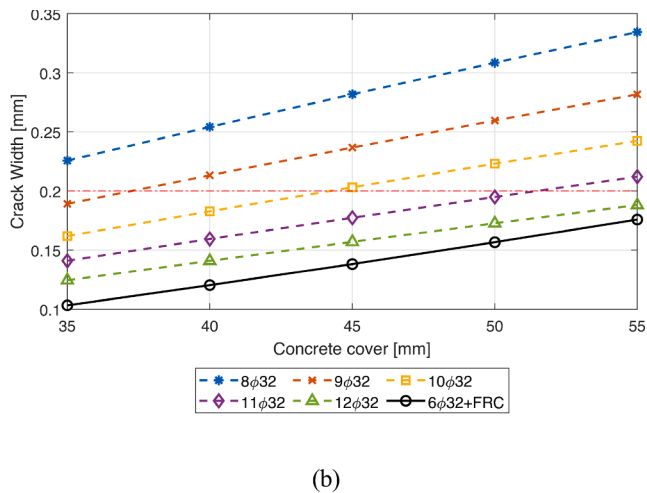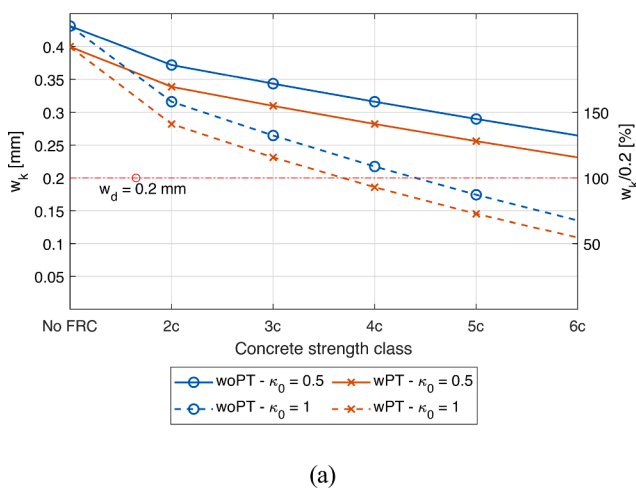
Fig. 11. Serviceability performance of FRC for the pier bottom slab. (a) Crack width reduction as a function of the concrete strength class and fiber orientation under the same performance requirement between cases, and (b) Crack width as a function of concrete cover and reinforcement quantity considering $\kappa_O = 1$ and for the woPT case. *Note: w_d is the design crack width limit.*

Table 7
ULS internal forces for shear verification at location 2 (Fig. 3). Axial compressive force is negative.

Case	ULS		
	N [kN/m]	V [kN/m]	M [kN/m]
woPT	164	64	152.4
wPT	−725	35	78.5

performance of FRC (measured as reinforcement substitution capabilities). However, the influence of FRC on reinforcement is based not only on the reinforcement quantity itself but also on the position of the rebars, specifically on their lever arm, as can be seen from Fig. 6a.

The fibers' effectiveness could then be measured in terms of the reinforcement ratio. It contains information about both reinforcement quantity and lever arm in a single parameter and serves as a direct measurement of the sectional capacity of the element. It should be noted that the effective depth indirectly defines the reinforcement lever arm, and thus, its position regarding the compressive resultant. At the same time, it defines most of the concrete area in the cross-section for rectangular elements, which participates as FRC enables a residual strength.

Fig. 10b shows how FRC performance, measured as ULS reinforcement reduction, can be related to the initial reinforcement ratio (considering an ordinary non-FRC solution) and in turn, related to the sectional mechanical capacity of the structural member. The efficiency of the fibers becomes more and more relevant as the bending requirement of the element becomes lower. Both Metrorreys' conventional solution and common reinforcement for building construction reinforcement ratios are close points to the complete elimination of reinforcement, being consistent with the results obtained in Section 4.1.1 and from previous literature (Section 1).

4.2.2. SLS verification with FRC

As already seen in Section 4.1.2, the use of fibers could reduce or eliminate the additional reinforcement specifically placed to ensure crack widths within code definitions while providing the same level of performance. As before and as a first tentative, the complete elimination of the additional reinforcement due to SLS (Table 6) is considered. Fig. 11a shows how a concrete strength class of 4c and beyond with $\kappa_O = 1$ can properly control the crack width. However, there is not any FRC strength class that can fulfill the crack opening limitation if $\kappa_O = 0.5$ and only the ULS reinforcement is present. Thus, for the pier segments, special care should be taken when defining the appropriate constitutive

Table 8
Stresses after ULS load combination for the wPT case at the mid-height of the web (in shell local coordinates) and transformation to principal stresses. *Notes: Compressions are negative. Element thickness of 30 cm. Element x direction matches the longitudinal axis of the bridge.*

Internal stresses in the element directions	σ_x [MPa]	σ_y [MPa]	τ_{xy} [MPa]
	−5.83	−3.2	3.66
Principal stresses	σ_1 [MPa]	σ_2 [MPa]	
	−5.83	−3.2	

Table 9
Concrete shear strength with conventional concrete (no FRC) compared to FRC 6c strength class. Reinforcement reduction if using FRC 6c. ($A_{s,w} = 18.7$ cm^2/m and $A_{s,w} = 11.5$ cm^2/m for the MC2010).

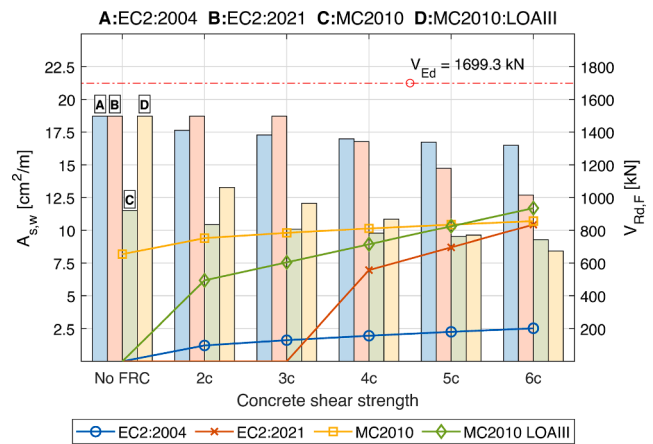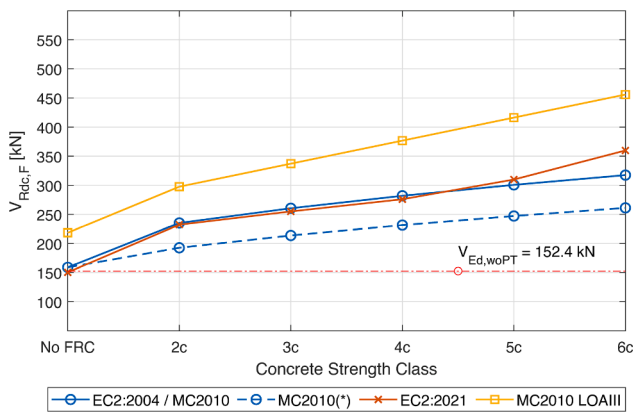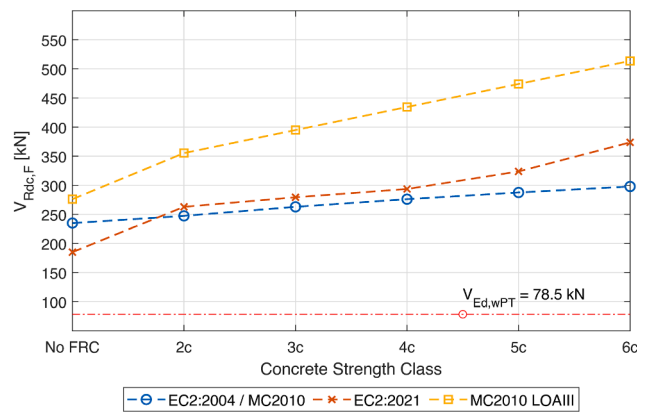|	MC2010	EC2:2004	EC2:2021	MC2010: LoAIII
Conventional concrete shear strength [kN/m]	654.3		469.2	367.6
FRC 6c shear strength [kN/m]	856.4		783.1	1029.5
Reinforcement reduction	19%	12%	32%	52%

Fig. 13. Required transversal reinforcement (bins, left axis) and concrete shear strength contribution, $V_{Rd,F}$ (lines with markers, right axis) compared to the design shear strength demand (V_{Ed}).

(a)

(b)

Fig. 12. Concrete shear strength without reinforcement for (a) woPT model case, and (b) wPT model case. The MC2010(*) verification uses the proposed coefficient $C_{Rd,c} = 0.15/\gamma_c$ from [42] and only affects FRC cases. The line-dot red line refers to the shear design internal force to be resisted (V_{Ed}). (For interpretation of the references to colour in this figure legend, the reader is referred to the web version of this article.)

law and casting procedures, as important deviations of the fibers' orientation could cause excessive crack widths.

It must be stressed that crack opening is not the only factor that affects durability but also the concrete cover. Although more and more owners require higher concrete covers to guarantee a long service life, increasing the concrete cover inevitably increases the crack width. Fig. 11b shows how increasing concrete cover requires higher amounts of reinforcement if the same rebar diameter is kept. The loads considered for the crack width obtention are from Table 2. For a concrete cover of 55 mm (rebar placed at 70 mm from the surface), the reinforcement requirement doubles with respect the reinforcement needed for ultimate resistance (6∅32 to 12∅32). Contrarily, it is possible to sustain admissible crack widths using FRC while keeping the ULS reinforcement (6∅32) no matter the concrete cover. For such high concrete covers, rebar meshes with low diameters could be placed to control cracking. However, with the use of FRC, those meshes could be suppressed as FRC can provide adequate crack control. The elimination of this skin reinforcement could lead to both labor reduction and an increase in casting ease and quality (as concrete has more room to flow between the formwork and the main reinforcement). According to [15,16], using FRC could effectively extend the service life of structures, including delayed corrosion-induced cracking and suppression of concrete spalling. Despite the potential serviceability improvements, a visual disadvantage should be noted when the bridge is accessible to the public at eyesight range. Uncoated steel fibers can produce superficial rust stains [40] that can bring in an unpleasant surface appearance. Beyond any aesthetics, the untrained public eye in front of FRC could misperceive rust stains as a sign of premature deterioration and possible loss of structural soundness. Regarding the prospective extension of the service life and corrosion-induced cracking, another issue to address is the adequate prediction of it for FRC. In that sense, tools and methods as the one presented in [41] are needed and must be calibrated for FRC to extend the long-term prediction capabilities for serviceability performance.

4.3. Shear verification

The shear verification is done utilizing four different formulations (although MC2010 and EC2:2004 share almost the same definition). However, the research does not aim to compare and analyze the differences and similarities between those formulations. These are used as a basis for consistency and the availability of tools that a designer could have during the design or assessment of a structure. The formulations used in the shear assessment, which must include the possible effect of fibers in concrete, are: 1) EC2:2004, 2) EC2:2021, 3) MC2010, and 4) MC2010:LoAIII (Level of Approximation III). The use of FRC in EC2:2004 is defined as per MC2010. As mentioned earlier, the expressions that the authors found contradictory are addressed in Section A.3. Some complementary expressions are obtained from [11]. Refer to Section A.3 for further details about the expressions and the assumed parameters for the bottom slab and web shear design.

4.3.1. Shear verification of the bottom slab – Midspan

The shear design of the bottom slab considers only the 30 cm deep slab as it is the slab thickness at the intersection with the web (see Fig. 1). The verification is done per unit width, and all the parameters used during shear calculations are shown in Table A3. The internal forces obtained from the numerical models in the transversal direction, both for the wPT and woPT analysis cases, are shown in Table 7.

Fig. 12 shows the concrete shear strength for both woPT and wPT cases. In all cases, the shear strength lies above the ultimate design load. Thus, the slabs verify the shear resistance without transversal reinforcement. However, as the bottom slab presents a one-way behavior, minimum shear reinforcement should be provided according to EC2, and is even more critical in this viaduct as segment joint opening is expected. The use of FRC would allow the elimination of such minimum

reinforcement, as pointed out in different design codes/recommendations. Hence, using FRC can provide a labor reduction regarding the intensive placing of transversal reinforcement.

In addition to the current design formulations, the observations made in [42,43] have been considered, where it was suggested that the current MC2010 could yield unsafe predictions for members not requiring transversal reinforcement. From [42], the coefficient $C_{Rd,c} = 0.18/\gamma_c$ from the concrete shear strength design formula of EC2:2004 and MC2010 is modified to $C_{Rd,c} = 0.15/\gamma_c$. From Fig. 12a, the MC2010 (*) check presents a constant reduction of 50 kN/m in the concrete shear strength when considering FRC.

The shear strengths from Fig. 12 are calculated including the longitudinal bending reinforcement from ULS values of Table 3. However, as seen in Fig. 6b, the conventional reinforcement can be suppressed if FRC 6c strength class is used in the wPT case. In that specific situation, the shear verification for FRC 6c strength class from Fig. 12b is no longer valid. It should be done by considering unreinforced/plain concrete design formulations and assuming f_{Ftuk} (characteristic ultimate residual strength of FRC at $w_u = 1.5$ mm) as the maximum tensile stress under principal stress directions. As a lower bound, disregarding the compressive stress of the transversal tendons, the shear stress obtained from the internal forces must be lower than the residual FRC strength to fulfill the shear design check. Provided that the cross-section is rectangular, the shear stress can be calculated as $\tau_{Ed} = 1.5 V_{Ed}/A_{cc} = 0.39$ MPa (shear design load and compressed concrete area respectively). As it is below f_{Ftuk}, the solution with only unbonded prestressing and fibers is still valid.

4.3.2. Shear verification of the webs

The cross-section considered for the longitudinal shear verification of the girder's webs lies approximately 3.2 m from the support axis, being entirely within the segment. The design is done for a single web, as a similar behavior is expected between webs, and it is only done within the segment but not at the joints. There is still no clear agreement on whether FRC can effectively improve the shear keys strength performance. According to Turmo et al. [44] and after their experimental campaign, the use of SFRC did not increase the shear capacity of the tested panels. However, other experimental campaigns had obtained different results [45]. Thus, it is assumed that the interface is designed as if it were a regular dry joint contact with conventional concrete (subsequently, out of the scope of this paper).

Each woPT and wPT cases is dealt with separately as the resisting mechanism differs depending on the existence or not of transverse post-tensioning. In the presence of transversal and longitudinal tendons (wPT case) the stress field at the web shifts from the common oblique compression-tension field to a biaxial compression state.

The shear strength verification for the wPT analysis is fulfilled by checking whether there are or are not principal tensile stresses in the concrete. If the transversal tendons are assumed to contribute to the girders' shear resistance, it must be imposed that no cracking can occur in the web and under any ULS load combination. Otherwise, once cracked, the unbonded nature of the post-tensioning could lead the web to an unpredictable failure (and most probably brittle).

The stresses from the web global coordinates are transformed to principal stresses as shown in Table 8. From the same table, the greater principal stress (σ_1) is in compression ($\sigma > 0 \equiv$ tension), thus verifying the shear requirement earlier stated (a biaxial compressive state is attained).

From the results of Table 8, no cracking is observed. However, if uncracked, FRC does not provide any benefit concerning the shear strength. In fact, any bridge that relies on vertical unbonded post-tension as the resisting mechanism for shear might not benefit from FRC as cracking should be avoided. It would be different if the webs were prestressed with bonded tendons (as in [22]).

Oppositely to wPT verification, the woPT shear check is done by means of conventional formulation, based on concrete, fibers, and

transversal reinforcement contributions to shear strength. The design loads for the shear verification of a single web are [N, M, V] = [−7384 kN, 1285 kNm, 1699 kN] (axial, bending and shear internal forces respectively).

Concrete crushing is not verified in detail as fibers do not explicitly modify its behavior from a code standpoint. However, previous FRC research in other areas but with similar load configurations indicates that concrete crushing after shear could benefit from fibers. Although focused on members purely under uniaxial compression, Paultre et al. [46] found that FRC could improve the overall ductility of the short columns and prevent premature spalling of the concrete cover. From [15], it was seen that flexural beams without fibers which failed due to concrete crushing (brittle failure) shifted their failure pattern to a more ductile one while maintaining the same ultimate strength if fibers were used. In fact, EC2:2021 allows FRC to endure larger ultimate compressive strains than regular reinforced concrete. Concerning bridge elements, post-tensioned members with high transversal reinforcement amounts could present a brittle compressive failure of the concrete strut under shear loading [47]. In these situations, FRC could arrest the brittleness of such failure by two different means: (1) FRC could reduce the vertical stresses that shear reinforcement induces to inclined concrete struts which, in turn, reduce the compressive concrete strength. Thus, increasing the strut compressive strength. And (2) FRC could improve the concrete spalling that occurs near heavily stressed regions. These improvements could optimize the web thickness when assessing shear. Currently, no code considers the improvement of the compressive strength of concrete in the struts due to shear as a function of the FRC strength class. Only MC2010 (LoAIII) allows the modification of the strut inclination if FRC is used, which increases the maximum allowable shear strength. However, this increase is not tied to the FRC strength class but rather to its mere existence.

The concrete shear strength and total shear resistance are computed following the expressions and parameters indicated in Table A4. These expressions assume that concrete has cracked, but highly prestressed members without expected flexure cracking should be verified through specific formulations for uncracked sections. However, according to [48], if simply supported post-tensioned girders have transversal reinforcement, it could be accepted to design shear assuming flexural cracks despite the high compressive forces.

Table 9 shows the computation of the concrete shear strength (without reinforcement) for both the conventional case (without FRC) and considering the FRC 6c class. No matter the FRC concrete strength and code formulation, the concrete shear strength does not reach the design shear load, and transversal reinforcement is always required. For the case of conventional concrete and disregarding the concrete contribution (as in EC2), 18.7 cm^2/m are needed to resist the shear design load (Fig. 13). In addition, the minimum transversal reinforcement requirement for the concrete strength class 6c can be obtained from Table 9 and Fig. 13.

From Fig. 13, the concrete shear contribution to overall resistance increases in all cases with the addition of fibers, although to a different extent depending on the formulation used. For EC2:2021, the strength increase is 50% from concrete strength class 4c to 6c. For lower FRC strength classes, the code formulation disregards the fiber contribution (and hence, any concrete contribution) as $V_{Rd} = \min\{V_{Rd,s}, \eta_s V_{Rd,s} + V_{Rd,FRC}\}$ (see Eq. (A8)).

MC2010 and EC2:2004 present the lower increase ratio when adding fibers, mostly because the FRC strength is not directly considered as it is in EC2:2021 and MC2010(LoAIII) but considered together with reinforcement ratio and concrete compressive strength. Such increase ranges from 14 to 30% for 2c to 6c FRC strength classes.

Despite the consistent increase of shear concrete contribution, especially for high FRC strength classes, Fig. 13 shows different reinforcement reductions between Model Code and Eurocode 2 formulations. This is not related to FRC calculations but to the fact that traditionally Eurocode 2 has disregarded the concrete contribution.

Thus, only the effect of fibers is captured in EC2 formulations rather than the effect of fibers and concrete together.

5. Conclusions

In this article, the use and potential benefits of FRC considered for the design of the Metrorrey Line 2 viaduct have been studied. Together with the existing viaduct and to extend the assessment to other similar wide U-shaped light-train viaducts, a transversely non-prestressed girder has also been studied. The study, which focused on structural performance, has shown that FRC participates in the load-bearing of the elements through (1) reinforcement replacement of cross-sections with initial low reinforcement ratios, (2) reduction of the serviceability-required reinforcement while providing same or lower crack width, and (3) increase in the shear strength of both bottom slab and webs, leading to reinforcement reductions of the webs transversal reinforcement.

Concerning the transversal bending and from an overall perspective, the use of FRC can be beneficial at two different levels. On the one hand, FRC can provide most of the required capacity to sustain ULS loads if relatively low internal force levels exist, almost replacing conventional reinforcement and providing enough bearing capacity. On the other hand, FRC will not offer any relevant optimization to the ULS reinforcement of members that undergo higher internal forces demands but will greatly influence (positively) their behavior under serviceability limit states.

Considering the Metrorrey existing viaduct, the transversal post-tensioning effect (if considered as an external load) on reducing the final internal forces on the slabs makes it possible to reach a low reinforcement ratio. Thus, the Metrorrey viaduct could be significantly benefited by FRC bearing capacity.

- In all cases, FRC allows for the reduction of reinforcement, whether it was required to fulfill ultimate or serviceability limitations.
- For similar viaducts to Metrorrey without transversal prestress, FRC can reduce the required reinforcement up to 16 and 33% of the initial ULS reinforcement for 25 and 35 cm thick slabs, respectively. FRC can completely eliminate the additional reinforcement for cracking control while reducing its width for high FRC strength classes.
- Fig. 10b can be a preliminary tool for assessing the FRC reinforcement reduction capacity under ULS combinations. FRC can reduce up to 50% of the initial reinforcement if $\rho_{s,Initial} \leq 0.4$. Oppositely, for ratios beyond 1% the benefits of FRC should be pointing towards SLS optimization criteria only, rather than ULS, as the reinforcement reduction reaches a horizontal asymptote near those reinforcement ratios.
- Regarding the current transversely post-tensioned solution of Metrorrey, the action of the tendons allows for very reduced reinforcement ratios. This classifies the section at the low end of Fig. 10b in terms of reinforcement ratios. Thus, the segment can take advantage of FRC in ULS by eliminating all the conventional reinforcement. The figure shows that Metrorrey segment slabs are at the boundary of maximum ULS reinforcement optimization. For increased internal forces the reinforcement reduction rapidly drops.
- Despite the full ULS reinforcement suppression is theoretically possible, rebar bands resembling APC reinforcement are still proposed to provide the minimum reinforcement, additional robustness, and local resistance. Construction-wise, these provide the physical support to set up the tendons and ducts. The use of bands gives more constructability freedom compared to traditional rebar cages, as they do not require special consideration for bar spacing and provide an easier and simpler reinforcement cage assembly. Oppositely to the transversal reinforcement, the longitudinal reinforcement of the bottom slab could be fully suppressed considering it is a secondary reinforcement. Fig. 7 shows the reinforcement proposal.

- Although using fibers does not offer an overall material saving, it could provide an overall cost reduction during construction. FRC allows part of the reinforcement to be suppressed, but the amount of fibers required for such reduction is usually higher than the original reinforcement weight itself. However, there is a noticeable reduction in labor as reinforcement layouts could be significantly simplified, pointing towards the overall cost reduction and increase in the construction quality.
- FRC 6c concrete strength class with an orientation factor $\kappa_O = 1$ has provided the means to entirely reduce the reinforcement required to fulfill serviceability crack width limitation if the concrete cover was increased. The material has been able to replace 12∅32 by 6∅32 (ULS reinforcement) while presenting a 55 mm concrete cover. However, further experimental investigation regarding the use of FRC with large concrete covers should be carried out as the calculations presented here are only based on design formulations. From past experiences (e.g. [16]), FRC can play an important role in terms of durability, which in turn can affect maintenance by potentially reducing it and the costs associated with it.

Regarding the verification of shear, all the formulations used, EC2:2004(+MC2010), EC2:2021, MC2010, and MC2010(LoAIII) can take advantage of FRC to enhance the concrete shear strength.

- For the shear design of the bottom slab in the transversal direction, the use of FRC increases about 50 to 75% of the shear strength of concrete, with similar order of magnitude compared to the bridge design from [24]. In the case of Metrorrey, the benefit is limited to the elimination of minimum reinforcement, if required.
- From Bairán et al. [42], a reduced coefficient for the MC2010 shear formulation for FRC has been used. The reduced coefficient has led to a sustained 50 kN/m reduction of the concrete shear strength. Although the reduction itself does not affect the verification of the current bottom slabs (the slabs did not require shear reinforcement in any configuration), the parameters update on the shear verification and regarding the prediction reliability could provide uncertainty and refrain the extension of FRC.
- Concerning the verification of reinforced concrete webs, FRC can increase the shear strength of concrete. However, as the shear demands are rather high for bridges, there is still a need for conventional shear reinforcement. Depending on the formulation, the benefit from FRC is greater or lower compared to the reinforcement reduction. In any case, reducing reinforcement could benefit congested areas in terms of transversal reinforcement.

- It should be pointed out the potential that FRC has for boosting the compressive strength of concrete in the struts due to shear. Not because of an increase in its bearing capacity but an improvement in the maximum strain it can endure and a reduction of the vertical strains due to shear reinforcement. This could turn a traditionally brittle failure into more ductile and provide means for possible web thickness reductions.

Regarding fatigue, the un-prestressed 25 cm bottom slab designed with FRC fulfills the required stress range limitation, even disregarding the bearing capacity of the fibers as the future EC2:2021 requires. Thus, the reduction of reinforcement favored by the use of FRC, from 8∅25 to 6∅25, is still valid after the fatigue check.

CRediT authorship contribution statement

Magí Domingo: Conceptualization, Methodology, Formal analysis, Investigation. **Gonzalo Ramos:** Conceptualization, Methodology, Supervision, Writing – review & editing, Project administration, Funding acquisition. **Ángel C. Aparicio:** Conceptualization, Methodology, Supervision, Writing – review & editing.

Declaration of Competing Interest

The authors declare that they have no known competing financial interests or personal relationships that could have appeared to influence the work reported in this paper.

Data availability

No data was used for the research described in the article.

Appendix A

A.1. Material properties

FRC tensile constitutive definitions: The bi-linear $\sigma - \varepsilon$ relationship from prEN1992-1-1:2021 is used to define the tensile branch of concrete, both for ULS and SLS considering the appropriate material partial safety factor. The required parameters are: $l_{cs} = 125$ mm, $w_u = 2.5$ mm, leading to $\varepsilon_{Ftu} = w_u/l_{cs} = 0.02$, together with the formulations from Table A1.

Mean crack spacing definitions according to prEN1992-1-1:2021: The cracking is calculated according to Eq. (A3) and with $k_b = 0.9$. The equation is taken from expression 9.19 of prEN1992-1-1:2021 (mean average crack space for regular concrete).

Table A1
Post-cracking strengths for design are as presented. It should be noted that those parameters might change after the draft discussion.

$w = 0.5$ mm	$w = 2.5$ mm
Stress-Strain Strength Parameters	
$f_{Ft1d} = \kappa_O \cdot 0.37 f_{R1,k}/\gamma_c$	$f_{Ft3d} = \kappa_O \cdot \left(0.57 f_{R3,k} - 0.26 f_{R1,k}\right)/\gamma_c$
Design Residual Tensile strengths	
$f_{Ftsd} = \kappa_O \cdot 0.4 \cdot f_{R1,k}/\gamma_c$	$f_{Ftud} = \kappa_O \cdot 0.37 f_{R3,k} \cdot \gamma_c$

Crack width is calculated as regular concrete (Eq. (A3)) but including the influence of FRC when calculating σ_s from sectional analysis, as well as including the parameter β_{FRC} in Eq. (A2).

$$\beta_{FRC} = 1 - \frac{f_{Ftsm}}{f_{ctm}} \text{ with } f_{Ftsm} = f_{Ftsk}/0.7 \tag{A1}$$

$$s_{r,m,cal} = 1.5 \cdot c + \frac{k_{fl} \cdot k_b}{7.2} \cdot \frac{\varnothing_{eq}}{\rho_{p,eff}} \cdot \beta_{FRC} \tag{A2}$$

$$w_k = 1.7 \cdot (\varepsilon_{sm} - \varepsilon_{cm}) \cdot s_{r,m,cal} \tag{A3}$$

Note: It has been considered f_{Ftsm} rather than f_{Ftsk} as it is consistent with MC2010 expressions.

A.2. Fatigue assumptions and calculations

Regarding the fatigue load assumptions, the following operational conditions are considered: 12 trains/h, 18 h/day, and 100% of operation during the year, the number of trains is roughly 79,000. If a 100-year service life is assumed, the total amount of loading cycles would be N = 7.9M $\approx 10^{6.898}$.

The maximum allowed reinforcement stress range is obtained from the EC2:2004 S—N curves (clause 6.8.4) and assuming that these are the only stress increments. Thus, from Eq. (A4) the stress range is obtained:

$$\log(\Delta\sigma_{Rsk}\gamma_{S,Fat}) = \left(-\frac{1}{k_2}\right)\log\left(\frac{N}{N^*}\right) + \log(\Delta\sigma_{Rsk}^*) \rightarrow \Delta\sigma_{Rsk} = 112.3 \text{ MPa} \tag{A4}$$

With $\gamma_{S,Fat} = 1.15$, $k_2 = 9$, $N^* = 10^6$ and $\Delta\sigma_{Rsk}^* = 162.5$ MPa.

A.3. Shear formulation - additional considerations

The formulations used to represent the different design codes are found in:

Shear formulation for prEN1992-1-1:2021: The shear formulation for EC2:2021 is taken as per Eqs. (A5)–(A8). The Eq. (A8) is defined from [11]. It must be stressed that the following formulation is obtained from a draft document, and therefore, it can change in future revisions. Nevertheless, the magnitude order that the presented formulas can lead is assumed to be correct.

$$\tau_{Rd,c} = \frac{0.66}{\gamma_V}\left(100 \cdot \rho_l \cdot f_{ck} \cdot \frac{d_{dg}}{d}\right)^{1/3} + k_1 \cdot \sigma_{cp} \tag{A5}$$

$$\tau_{Rd,F} = \eta_C \cdot \tau_{Rd,c} + f_{Ftud} \tag{A6}$$

$$\tau_{Rd,s} = \frac{A_{sw}}{b_w \cdot s} \cdot f_{yd,w} \cdot \cos\theta \tag{A7}$$

$$\tau_{Rd,sF} = (\eta_s \cdot \tau_{Rd,s}/\cos\theta + f_{Ftud}) \cdot \cos\theta \geq \tau_{Rd,s} \tag{A8}$$

With $\eta_C = \max(1/(1 + 0.43 \cdot f_{Ftuk}^{2.85}), 0.4)$, $\eta_s = 0.75$ and $\sigma_{cp} > 0$ for axial compression (see Table A2).

Longitudinal strain ε_x in Model Code 2010 – LoAIII: As the train plane due to axial-bending loads can be accurately known, the longitudinal strain used to compute the shear strength according to Model Code 2010 is considered as in Eq. (A9). This is consistent with the formulation provided in expressions 7.3–14 and 7.3–16 from Section 7.3.3 of Model Code 2010, where longitudinal strain due to shear is included.

Table A2
Reference to code formulations used for the shear strength analysis.

EN1992-1-1:2004	Section 6.2 of the code with additional considerations from section 7.7.3.2 from Model Code 2010 Vol.2
Model Code 2010	Section 7.7.3.2 from Model Code 2010 Vol.2
Model Code 2010 - LoAIII	Section 7.3.3 for regular concrete formulation together with Section 7.7.3.2

$$\varepsilon_x = \varepsilon_{x,b} + \frac{V_{Ed}}{2E_s A_s} \tag{A9}$$

Where $\varepsilon_{x,b}$ is the longitudinal strain at $z/2$ due to axial and bending loads.
Table A3 and Table A4 show the parameters considered for the shear computations.

Table A3
Parameters for the shear strength of the slab. The symbols are adopted from each code formulation.

Common parameters	h = 300 mm, d = 250 mm, z = 0.9d, b = 1000 mm, $\theta = 45°$, $A_c = h \bullet b$, $f_{yd,w} = 500/1.15$ MPa and $A_{sl} = 4\varnothing25$ (woPT case)/$4\varnothing12$ (wPT case) f_{Ftuk} at w = 1.5 mm for EC2:2004, MC2010 and MC2010-LoAIII
EC2:2021 Parameters	$d_{dg} = 32$ mm, $\gamma_V = 1.4$, $k_1 = 0.15$
MC2010 Parameters	$k_{dg} = 0.889$, $\varepsilon_{x,b} = 3.9473e^{-4}/-1.0763e^{-4}$ for woPT/wPT cases respectively.

Table A4

Parameters for the shear strength of the webs. The symbols are adopted from each code formulation.

Common parameters	h = 1900 mm, d = 1775 mm, z = 1430 mm, b = 300 mm, $\theta = 35°$, $A_c = 1.0379e^6$ mm2, $f_{yd,w} = 500/1.15$ MPa and $A_{sl} = 2550$ mm^2
	f_{Ftuk} at $w = 1.5$ mm for EC2:2004, MC2010 and MC2010-LoAIII
EC2:2021 Parameters	$d_{dg} = 32$ mm, $\gamma_V = 1.4$, $k_1 = 0.15$
MC2010 Parameters	$k_{dg} = 0.889$, $\varepsilon_{x,b} = -3.353e^{-3}$, $A_s = 10200$ mm2 for ε_x computation.

References

[1] ACI Committee 544. 544.1R-96: report on fiber reinforced concrete (Reapproved 2009). American Concrete Institute; 2019.

[2] di Prisco M, Plizzari G, Vandewalle L. Fibre reinforced concrete: new design perspectives. Mater Struct 2009;42(9):1261–81. https://doi.org/10.1617/s11527-009-9529-4.

[3] Soranakom C, Mobasher B. Flexural design of fiber-reinforced concrete. ACI Mater J 2009;106(5):461–9. https://doi.org/10.14359/51663147.

[4] Li VC. Large volume, high-performance applications of fibers in civil engineering. J Appl Polym Sci 2002;83(3):660–86. https://doi.org/10.1002/app.2263.

[5] Serna P, Arango S, Ribeiro T, Núñez AM, Garcia-Taengua E. Structural cast-in-place SFRC: technology, control criteria and recent applications in Spain. Mater Struct 2009;42(9):1233–46. https://doi.org/10.1617/s11527-009-9540-9.

[6] di Prisco M, Colombo M, Pourzarabi A. Biaxial bending of SFRC slabs: is conventional reinforcement necessary? Mater Struct 2019;52(1):1. https://doi.org/10.1617/s11527-018-1302-0.

[7] Maturana A, Canales J, Orbe A, Cuadrado J. Análisis plástico y Ensayos de Losas multidireccionales de HRFA. Inf. la Construcción 2014;66(535):e031. doi: 10.3989/ic.13.021.

[8] Destrée X. Steel fiber-reinforced concrete in free suspended-elevated slabs. In: SP-268: fiber reinforced concrete in practice; 2010. p. 155–64. doi: 10.14359/51663715.

[9] Aidarov S, Mena F, de la Fuente A. Structural response of a fibre reinforced concrete pile-supported flat slab: full-scale test. Eng Struct 2021;239:112292. https://doi.org/10.1016/j.engstruct.2021.112292.

[10] Amin A, Foster SJ. Shear strength of steel fibre reinforced concrete beams with stirrups. Eng Struct 2016;111:323–32. https://doi.org/10.1016/j.engstruct.2015.12.026.

[11] Minelli F, Plizzari GA. Shear strength of FRC members with little or no shear reinforcement: a new analytical model; 2010. doi: 10.35789/fib.bull.0057.ch13.

[12] Soetens T, Matthys S, Hertelé S, De Waele W. Shear behaviour of prestressed precast SFRC girders. Eng Struct 2017;142:20–35. https://doi.org/10.1016/j.engstruct.2017.03.069.

[13] Cuenca E, Serna P. Shear behavior of prestressed precast beams made of self-compacting fiber reinforced concrete. Constr Build Mater 2013;45:145–56. https://doi.org/10.1016/j.conbuildmat.2013.03.096.

[14] Gholamhoseini A, Khanlou A, MacRae G, Scott A, Hicks S, Leon R. An experimental study on strength and serviceability of reinforced and steel fibre reinforced concrete (SFRC) continuous composite slabs. Eng Struct 2016;114:171–80. https://doi.org/10.1016/j.engstruct.2016.02.010.

[15] Berrocal CG, Löfgren I, Lundgren K. The effect of fibres on steel bar corrosion and flexural behaviour of corroded RC beams. Eng Struct 2018;163:409–25.

[16] Berrocal CG. Corrosion of steel bars in fibre reinforced concrete: corrosion mechanisms and structural performance. Chalmers University of Technology; 2017.

[17] Mufti AA, Jaeger LG, Baidar B, Wegner LD. Experimental investigation of fibre-reinforced concrete deck slabs without internal steel reinforcement. Can J Civ Eng 1993;20(3):398–406. https://doi.org/10.1139/l93-055.

[18] Massicotte B, Cordoni N. Design of precast prestressed SFRC T-girders for accelerated sustainable bridge construction. In: Massicotte B, Minelli F, Mobasher B, Plizzari G, editors. Fibre reinforced concrete: from design to structural applications. Proceedings of the ACI-fib-RILEM international workshop - FRC2018, Vol. 343; 2020. p. 195–204.

[19] Massicotte B, Bélanger A, Moffatt K. Analysis and design of SFRC bridge decks. In: 5th RILEM symposium on fibre-reinforced concretes (FRC); 2000. p. 263–72 [Online]. Available: https://www.rilem.net/publication/publication/20?id_papier=1650.

[20] McMahon JA, Birely AC. Experimental performance of steel fiber reinforced concrete bridge deck. J Bridg Eng 2018;23(10):04018074. https://doi.org/10.1061/(asce)be.1943-5592.0001287.

[21] Birely AC, Park P, McMahon JA, Shi X, Rew Y. SPR-705: fiber-reinforced concrete for the improved performance of transportation infrastructure; 2018 [Online]. Available: https://rosap.ntl.bts.gov/view/dot/37207.

[22] Kasuga A. Effects of butterfly web design on bridge construction. Struct Concr 2017;18(1):128–42. https://doi.org/10.1002/suco.201600109.

[23] Shibata T, Kata K, Kasuga A, Sakai K. Sustainability evaluation of butterfly web bridge. Struct Concr 2018;19(2):422–39. https://doi.org/10.1002/suco.201700010.

[24] Winkler A, Edvardsen C, Kasper T. Examples of bridge, tunnel lining and foundation design with steel-fibre-reinforced concrete. In: Fibre-reinforced concrete: from design to structural applications. FRC 2014: joint ACI-fib International Workshop; May 2016. p. 451–60. doi: 10.35789/fib.BULL.0079.Ch42.

[25] Baamonde JJG, y Benitez AMG. Metrorrey's linea 2 extension viaduct: a revolution for light-rail precast concrete segmental bridges. PCI J 2009;54(4):175–88. doi: 10.15554/pcij.09012009.175.188.

[26] CEN. EN1991-2:2003 - Eurocode 1: actions on structures - Part 2: traffic loads on bridges; 2003.

[27] CEN. EN1992-1-1:2004 - Eurocode 2: design of concrete structures - Part 1-1 : general rules and rules for buildings; 2004.

[28] CEN. prEN1992-1-1:2021-09 - Eurocode 2: design of concrete structures - Part 1-1: general rules - rules for buildings, bridges and civil engineering structures (DRAFT); 2021.

[29] Fédération Internationale du Béton (fib). fib Bulletin 65. Model code 2010 Volume 1. fib. The International Federation for Structural Concrete; 2012.

[30] Fédération Internationale du Béton (fib). fib Bulletin 66. Model Code 2010 Volume 2. fib. The International Federation for Structural Concrete; 2012.

[31] MITMA. AN/UNE-EN 1992-1-1 - Anejo Nacional Eurocódigo 2: Proyecto de estructuras de hormigón. Parte 1-1: Reglas generales y reglas para edificación; 2015.

[32] Computers & Structures Inc. CSI Analysis Reference Manual - SAP2000 v21; 2017.

[33] ACI Committee 318. 318-19: building code requirements for structural concrete and commentary. American Concrete Institute; 2019.

[34] ACI-ASCE Committee 423. 423.3R-17: Recommendations for concrete members prestressed with single-strand unbonded tendons; 2017.

[35] Mitchell D, Cook WD. Preventing progressive collapse of slab structures. J Struct Eng 1984;110(7):1513–32. https://doi.org/10.1061/(ASCE)0733-9445(1984)110:7(1513).

[36] CNR - Consiglio Nazionale delle Ricerche. CNR-DT 204/2006: Istruzioni per la Progettazione, l'Esecuzione ed il Controllo di Strutture di Calscestruzzo Fibrorinforzato; 2006.

[37] Isojeh B. Fatigue damage analysis of reinforced concrete structural elements. University of Toronto; 2017.

[38] Germano F, Tiberti G, Plizzari G. Post-peak fatigue performance of steel fiber reinforced concrete under flexure. Mater Struct 2016;49(10):4229–45. https://doi.org/10.1617/s11527-015-0783-3.

[39] Rivera M, Enfedaque A, Alberti MG, Gálvez JC, Simón-Talero JM. Crack-width-based sectional analysis of fiber-reinforced concrete applied to the structural design of the slab of a fly-over Bridge. J Bridg Eng 2022;27(1):1–16. https://doi.org/10.1061/(ASCE)BE.1943-5592.0001793.

[40] Serna P, Arango SE. Evolution of the flexural behavior of precracked SFRC in marine environment. In: 7th RILEM international symposium on fibre reinforced concrete: design and applications - BEFIB 2008, Vol. 20, no. 5; 2008. p. 1103–9.

[41] Chen S, Duffield C, Miramini S, Nasim Khan Raja B, Zhang L. Life-cycle modelling of concrete cracking and reinforcement corrosion in concrete bridges: a case study. Eng Struct 2021;237:112143.

[42] Bairán JM, Tošić N, de la Fuente A. Reliability-based assessment of the partial factor for shear design of fibre reinforced concrete members without shear reinforcement. Mater Struct 2021;54(5):185. https://doi.org/10.1617/s11527-021-01773-z.

[43] Soetens T. Design models for the shear strength of prestressed precast steel fibre reinforced concrete girders. Ghent University; 2015.

[44] Turmo J, Ramos G, Aparicio ÁC. Shear strength of dry joints of concrete panels with and without steel fibres. Eng Struct 2006;28(1):23–33. https://doi.org/10.1016/j.engstruct.2005.07.001.

[45] Jiang H, Wei R, John Ma Z, Li Y, Jing Y. Shear strength of steel fiber-reinforced concrete dry joints in precast segmental bridges. J Bridg Eng 2016;21(11):1–13. https://doi.org/10.1061/(ASCE)BE.1943-5592.0000968.

[46] Paultre P, Eid R, Langlois Y, Lévesque Y. Behavior of steel fiber-reinforced high-strength concrete columns under uniaxial compression. J Struct Eng 2010;136(10):1225–35. https://doi.org/10.1061/(ASCE)ST.1943-541X.0000211.

[47] Aparicio ÁC, Calavera J, del Pozo FJ. Investigación sobre la compresión máxima en bielas por esfuerzo cortante en piezas prefabricadas de hormigón pretensado con armaduras pretesas. Available: Hormigón y Acero 1998;49(209):33–45. http://www.hormigonyacero.com/index.php/ache/article/view/421.

[48] Marí A, Bairán JM, Cladera A, Oller E. Shear design and assessment of reinforced and prestressed concrete beams based on a mechanical model. J Struct Eng 2016;142(10). https://doi.org/10.1061/(ASCE)ST.1943-541X.0001539.